Supporting Information

High-Throughput Screening for Efficient Dual-Atom Catalysts in Electrocatalytic Nitrate Reduction to Ammonia via Dissociation-Association Mechanism

*Lingling Lv,[1, †] Yanqing Shen,[1,3, †, *] Min Zhou,[1] Yu Zhang,[1] Xianghui Meng,[1] Xin Yang,[1] Nan Zhang,[1] Kexin Wang,[1] Qirui He,[1] Dewei Gong,[1,3], Qing Ai,[2, *] Yong Shuai,[2, *] Zhongxiang Zhou[1,3, *]*

1 School of Physics, Harbin Institute of Technology, Harbin 150001, PR China

2 School of Energy Science and Engineering, Harbin Institute of Technology, Harbin, 150001, PR China

3 Heilongjiang Provincial Key Laboratory of Plasma Physics and Application Technology, Harbin Institute of Technology, Harbin 150001, PR China

† Contributed equally to this work

* Corresponding authors: Yanqing Shen. E-mail: shenyanqing2004@163.com

Qing Ai, E-mail: hitaiqing@hit.edu.cn

Yong Shuai, E-mail: shuaiyong@hit.edu.cn

Zhongxiang Zhou. E-mail: zhouzx@hit.edu.cn

COMPUTATIONAL METHOD

In the path of NO_3RR to ammonia (NH_3), 9 protons and 8 electrons are transferred. The whole reaction can be summarized as $NO_3^- + 9H^+ + 8e^- \rightarrow NH_3 + 3H_2O$ [1]. Firstly, nitrate will be adsorbed on M1M2/g-C_3N_4, the equation is as follows (In which * represents M1M2/g-C_3N_4 substrates, *NO_3 represents NO_3^- adsorption on M1M2/g-C_3N_4 substrate, *M represents the intermediate products M adsorption on M1M2/g-C_3N_4 substrate):

$$*+NO_3^- \rightarrow *NO_3 + e^- \quad \text{(S1)}$$

After the *NO_3, the first fork in the reaction path will appear, the *NO_3H (equation S2, S3) or *NO_2 (equation S4) will be generated:

$$*NO_3 + H^+ + e^- \rightarrow *NO_3H \quad \text{(S2)}$$

$$*NO_3H + H^+ + e^- \rightarrow *NO_2 + H_2O \quad \text{(S3)}$$

Or $$*NO_3 + 2H^+ + 2e^- \rightarrow *NO_2 + H_2O \quad \text{(S4)}$$

After the *NO_2, the second fork in the reaction path will appear, the *NO_2H (equation S5, S6) or *NO (equation S7) will be generated:

$$*NO_2 + H^+ + e^- \rightarrow *NO_2H \quad \text{(S5)}$$

$$*NO_2H + H^+ + e^- \rightarrow *NO + H_2O \quad \text{(S6)}$$

Or $$*NO_2 + 2H^+ + 2e^- \rightarrow *NO + H_2O \quad \text{(S7)}$$

After the *NO_2, *NOH will be generated:

$$*NO + H^+ + e^- \rightarrow *NOH \quad \text{(S8)}$$

After the *NOH, the third fork in the reaction path will appear, the *NHOH (equation S9) or *N (equation S10) will be generated:

$$*NOH + H^+ + e^- \rightarrow *HNOH \quad \text{(S9)}$$

Or $$*NOH + H^+ + e^- \rightarrow *N + H_2O \quad \text{(S10)}$$

Whether for the *NHOH (equation S11) or *N (equation S12), the next step the *NH will be generated:

$$*HNOH+H^+ + e^- \rightarrow *NH+H_2O \quad (S11)$$

Or $$*N+H^+ + e^- \rightarrow *NH \quad (S12)$$

After *NH, NH_3 will be generated progressively:

$$*NH+H^+ + e^- \rightarrow *NH_2 \quad (S13)$$

$$*NH_2+H^+ + e^- \rightarrow *NH_3 \quad (S14)$$

$$*NH_3 \rightarrow *+NH_3 \quad (S15)$$

NO may be produced after the *NO of the reaction of NO_3RR to NH_3:

$$*NO \rightarrow *+NO \quad (S16)$$

NO may be produced after the $*NO_2$ of the reaction of NO_3RR to NH_3:

$$*NO_2 \rightarrow *+NO_2 \quad (S17)$$

N_2 may be produced after the *NO of the reaction of NO_3RR to NH_3:

$$*NO+*NO \rightarrow *N_2O_2 \quad (S18)$$

$$*N_2O_2+H^+ + e^- \rightarrow *N_2O_2H \quad (S19)$$

$$*N_2O_2H+H^+ + e^- \rightarrow *N_2O+H_2O \quad (S20)$$

$$*N_2O+H^+ + e^- \rightarrow *N_2OH \quad (S21)$$

$$*N_2OH+H^+ + e^- \rightarrow *N_2+H_2O \quad (S22)$$

$$*N_2 \rightarrow *+N_2 \quad (S23)$$

N_2 also may be produced after the *N of the reaction of NO_3RR to NH_3:

$$*N+*N \rightarrow * + *N_2 \quad (S24)$$

The potential limiting steps of the NO_3RR to NH_3 reaction are $*NO+H^+ + e^- \rightarrow *NOH$ and $*NH_2+H^+ + e^- \rightarrow *NH_3$, which determine whether the M1M2/g-C_3N_4 can perform the NO_3RR to NH_3 reaction. Limiting potential required for the reaction can be determined by calculating the Gibbs free energy in both steps: U_L =

$-\Delta G_{Max}$/e, in which ΔG_{Max} is the maximum value for each order of free energy change.

The Gibbs free energy change ΔG are calculated according to the computational hydrogen electrode (CHE) model proposed by Nørskov et al: [2]

$$\Delta G = \Delta E + \Delta E_{ZPE} - T\Delta S + \Delta G_U \quad \text{(S25)}$$

where ΔE represents the change of total energy of the intermediate before and after adsorption, ΔE_{ZPE} and $T\Delta S$ are the zero-point energy difference and the entropy, respectively. $\Delta G_U = -eU$ represents the influence of electrode potential on ΔG.

The adsorption energy of NO_3^- on M1M2/g-C_3N_4 substrate is calculated with $\Delta G_{*NO_3} = G_{*NO_3} - G_* - G_{HNO_3(g)} + 0.5G_{H2(g)} + \Delta G_{correct}$, in which G_{*NO3} and G_* represent the energy of M1M2/g-C_3N_4 with anchored NO_3^- and pure M1M2/g-C_3N_4, $G_{HNO3(g)}$ and $G_{H2(g)}$ express the energy of HNO_3 and H_2 molecules in the gas phase, $\Delta G_{correct} = 0.392$ eV. [2]

The transition state is completed with the complete LST/QST method. The spin-polarized AIMD (ab initio molecular dynamic) simulation under a constant volume and temperature (NVT) ensemble are fulfilled using the Dmol3 package [3], and the initial temperature is set to 300 K and 800 K.

An implicit water solvent environment is simulated in the Dmol3 package, which includes certain the conductor-like screening model (COSMO) controls that can be used to simulate a solvent environment for the calculation [4,5]. Core electrons are processed with All Electrons and the double numerical plus polarization (DNP) is used as the basis set. 3×3×1 k-point grids, which the same as in the case of CASTEP, is selected. The

DFT-D and spin-polariton are also applied.

When calculating the Surface Pourbaix diagrams [6], the following hydrolysis reactions are taken into account:

$$*O_mH_n + (2m\text{-}n)(H^+ + e^-) \rightarrow * + mH_2O \quad \text{(S26)}$$

where m and n are the number of oxygen and hydrogen atoms of the adsorbate, respectively. The free energy changes involving electric potential and pH are calculated using:

$$\Delta G = G_* + m\,G_{H_2O} - G_{*OmHn} - (2\,m - n)(0.5G_{H_2} - U_{SHE} - 2.303k_B T\,pH) \quad \text{(S27)}$$

where U_{SHE} is the potential relative to the standard hydrogen electrode (SHE), k_B is the Boltzmann constant (8.617343×10^{-5} eV K^{-1}), T is the temperature.

RESULTS AND DISCUSSIONS

Table S1. The formation energy E_f and dissolution potential U_{diss} of M1M2/g-C_3N_4

	E_f	U^0_{diss}(metal,bulk)	N_e	U_{diss}
TiTi	−3.06	−1.63	2	−0.10
TiV	−2.86	−1.41	2	0.03
TiCr	−4.10	−1.27	2	0.78
TiMn	−2.90	−1.41	2	0.04
TiFe	−3.08	−1.04	2	0.50
TiCo	−2.95	−0.96	2	0.52
TiNi	−3.82	−0.95	2	0.96
TiCu	−5.04	−0.65	2	1.87
VV	0.36	−1.18	2	−1.36
VCr	−3.23	−1.04	2	0.57
VMn	0.54	−1.19	2	−1.45
VFe	−1.82	−0.82	2	0.09
VCo	−2.06	−0.73	2	0.30
VNi	−3.40	−0.72	2	0.98
VCu	−3.91	−0.42	2	1.54
CrCr	−4.01	−0.91	2	1.09
CrMn	−3.04	−1.05	2	0.47
CrFe	−3.09	−0.68	2	0.87
CrCo	−3.32	−0.60	2	1.07

CrNi	−4.55	−0.59	2	1.69
CrCu	−4.45	−0.29	2	1.94
MnMn	3.57	−1.19	2	−2.97
MnFe	−1.28	−0.82	2	−0.18
MnCo	−1.51	−0.74	2	0.02
MnNi	−3.16	−0.73	2	0.86
MnCu	−3.12	−0.43	2	1.13
FeFe	−1.23	−0.45	2	0.17
FeCo	−1.12	−0.37	2	0.20
FeNi	−1.99	−0.36	2	0.64
FeCu	−2.70	−0.01	2	1.29
CoCo	−0.62	−0.28	2	0.03
CoNi	−1.66	−0.27	2	0.56
CoCu	−2.12	0.03	2	1.09
NiNi	−3.45	−0.26	2	1.47
NiCu	−2.65	0.04	2	1.37
CuCu	−2.87	0.34	2	1.77

Table S2. The computation details for calculating the potential determining steps ΔG*NO-*NOH, ΔG*NH_2-*NH_3, limiting potentials U_L, G_{*NO3} and G_{*H}.

	ΔG*NO-*NOH	ΔG*NH_2-*NH_3	U_L (V)	ΔG_{*NO3}	ΔG_{*H}
TiV	2.23	0.78	−2.23	−2.76	−0.85
TiCr	1.08	0.69	−1.08	−2.28	−1.28
TiMn	0.61	0.50	−0.61	−1.88	−0.44
TiFe	0.04	0.21	−0.21	−2.38	−0.77
TiCo	0.16	0.56	−0.56	−2.46	−0.78
TiNi	0.10	0.88	−0.88	−1.85	−0.76
TiCu	0.42	−0.05	−0.42	−0.98	0.23
VCr	0.77	0.81	−0.81	−1.74	−1.04
VFe	0.38	0.62	−0.62	−2.09	−0.80
VCo	0.25	0.74	−0.74	−2.18	−0.66
VNi	0.57	1.14	−1.14	−1.32	−0.80
VCu	1.23	0.20	−1.23	−0.69	0.06
CrCr	0.61	0.16	−0.61	−1.54	0.06
CrMn	0.65	0.67	−0.67	−1.72	−1.17
CrFe	1.02	0.89	−1.02	−1.13	−1.10
CrCo	1.15	0.67	−1.15	−0.96	−0.83
CrNi	0.81	0.56	−0.81	−0.77	−1.10
CrCu	0.78	0.40	−0.78	−1.63	−1.14
MnCo	0.92	0.25	−0.92	−1.63	−0.65

MnNi	0.68	−0.34	−0.68	−0.35	−0.54
MnCu	−0.09	0.82	−0.82	−1.28	−1.06
FeFe	0.77	−0.25	−0.77	−1.80	−0.70
FeCo	0.58	0.17	−0.58	−1.64	−0.72
FeNi	0.54	0.20	−0.54	−1.22	−0.64
FeCu	0.37	0.15	−0.37	−0.92	−0.84
CoCo	−0.15	0.75	−0.75	−1.67	−1.44
CoNi	0.54	0.77	−0.77	−0.96	−0.54
CoCu	0.69	0.59	−0.69	−1.04	−1.24
NiNi	0.74	−0.63	−0.74	0.68	−0.55
NiCu	−0.21	0.32	−0.32	−0.86	−0.75
CuCu	0.65	0.82	−0.82	−1.78	−1.20

Table S3. The adsorption energies of nitrate on the 2O-end configurations: position 1, position 2, position 3 and the 1O-end configurations (position marked on red) of M1M2/g-C_3N_4, in which the red color represents the most stable adsorption configuration.

	1-ΔG_{*NO3}	2-ΔG_{*NO3}	3-ΔG_{*NO3}	1-O end-ΔG_{*NO3}	ΔG_{*NO3}
TiV	−2.69	−1.93	−2.76	−2.28	−2.76
TiCr	−2.21	−1.62	−2.28	−1.58	−2.28
TiMn	−1.88	−1.70	−1.65	−1.30	−1.88
TiFe	−2.11	−1.83	−2.38	−1.62	−2.38
TiCo	−1.86	−2.05	−2.46	−1.54	−2.46
TiNi	−1.37	−1.57	−1.85	−0.65	−1.85
TiCu	−0.25	−0.98	−0.11	0.24	−0.98
VCr	−1.74	−1.56	−1.64	−1.31	−1.74
VFe	−2.01	−1.89	−2.09	−1.57	−2.09
VCo	−1.76	−1.74	−2.18	−1.35	−2.18
VNi	−0.74	−0.98	−1.32	−0.35	−1.32
VCu	−0.17	−0.69	0.06	0.36	−0.69
CrCr	−0.93	−1.54	−1.04	−0.50	−1.54
CrMn	−1.56	−1.72	−1.47	−0.91	−1.72
CrFe	−1.13	−0.80	−1.06	−0.49	−1.13
CrCo	−0.91	−0.96	−0.85	−0.55	−0.96
CrNi	4.83	−0.40	−0.77	−0.35	−0.77
CrCu	−1.39	−0.94	−1.63	−1.17	−1.63
MnCo	−1.58	−0.65	−1.63	−1.19	−1.63

MnNi	−0.35	−0.08	−0.33	−0.32	−0.35
MnCu	−1.28	−0.97	−0.86	−0.92	−1.28
FeFe	−1.80	−1.13	−1.75	−1.36	−1.80
FeCo	−1.64	−1.57	−1.58	−1.28	−1.64
FeNi	−1.10	−0.62	−1.22	−0.77	−1.22
FeCu	−0.89	−0.80	−0.92	−0.66	−0.92
CoCo	−1.67	−0.49	3.99	4.22	−1.67
CoNi	−0.96	−0.55	−0.55	5.01	−0.96
CoCu	−0.95	−0.55	−1.04	−0.62	−1.04
NiNi	0.68	1.27	0.92	1.64	0.68
NiCu	−0.73	−0.86	5.40	4.69	−0.86
CuCu	−0.76	−0.47	−1.78	−0.10	−1.78

Table S4. Comparisons of Gibbs free energies for the potential-determining steps without and with solvation for TiFe/g-C_3N_4, FeCu/g-C_3N_4 and NiCu/g-C_3N_4.

	ΔG*NO-*NOH (without sol)	ΔG*NO-*NOH (with sol)	ΔG*NH_2-*NH_3 (without sol)	ΔG*NH_2-*NH_3 (with sol)
TiFe	0.04	0.004	0.21	−0.30
FeCu	0.37	0.47	0.15	−0.10
NiCu	−0.21	−0.21	0.32	0.36

Table S5. The catalytic performance of TiFe/g-C_3N_4 catalysts with different N atomic number coordination are also considered. By changing the number of N atoms around TiFe bimetallic atoms, the regulatory effect of microenvironment changes on the catalytic performance of TiFe/g-C_3N_4 dual atom catalysts are explored. From the table below, it can be seen that TiFe/g-C_3N_4 catalyst with 6 N atom number coordination shows the best catalytic performance (0.21 eV). As the number of N atoms gradually decreases, the stronger its adsorption effect on nitrate (TiFe-5N/g-C_3N_4: −2.59 eV; TiFe-5N/g-C_3N_4: −2.72 eV), the greater the Gibbs free energy of its potential determining step (TiFe-5N/g-C_3N_4: 0.80 eV; TiFe-5N/g-C_3N_4: 0.88 eV), which means that its catalytic performance is getting worse and worse.

	ΔG*NO_3	ΔG*NO-*NOH	ΔG*NH_2-*NH_3
TiFe-6N	−2.38	0.04	0.21
TiFe-5N	−2.59	0.71	0.80
TiFe-4N	−2.72	0.88	0.24

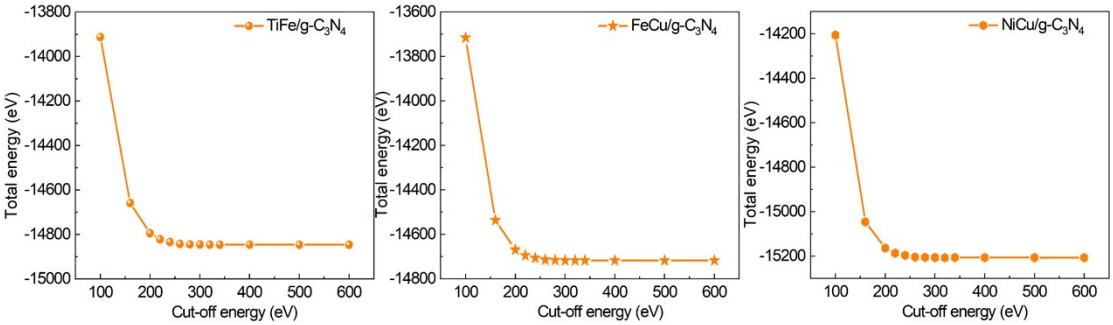

Figure S1 In order to select a suitable cut-off energy, convergence tests for TiFe/g-C_3N_4, FeCu/g-C_3N_4 and NiCu/g-C_3N_4 are performed.

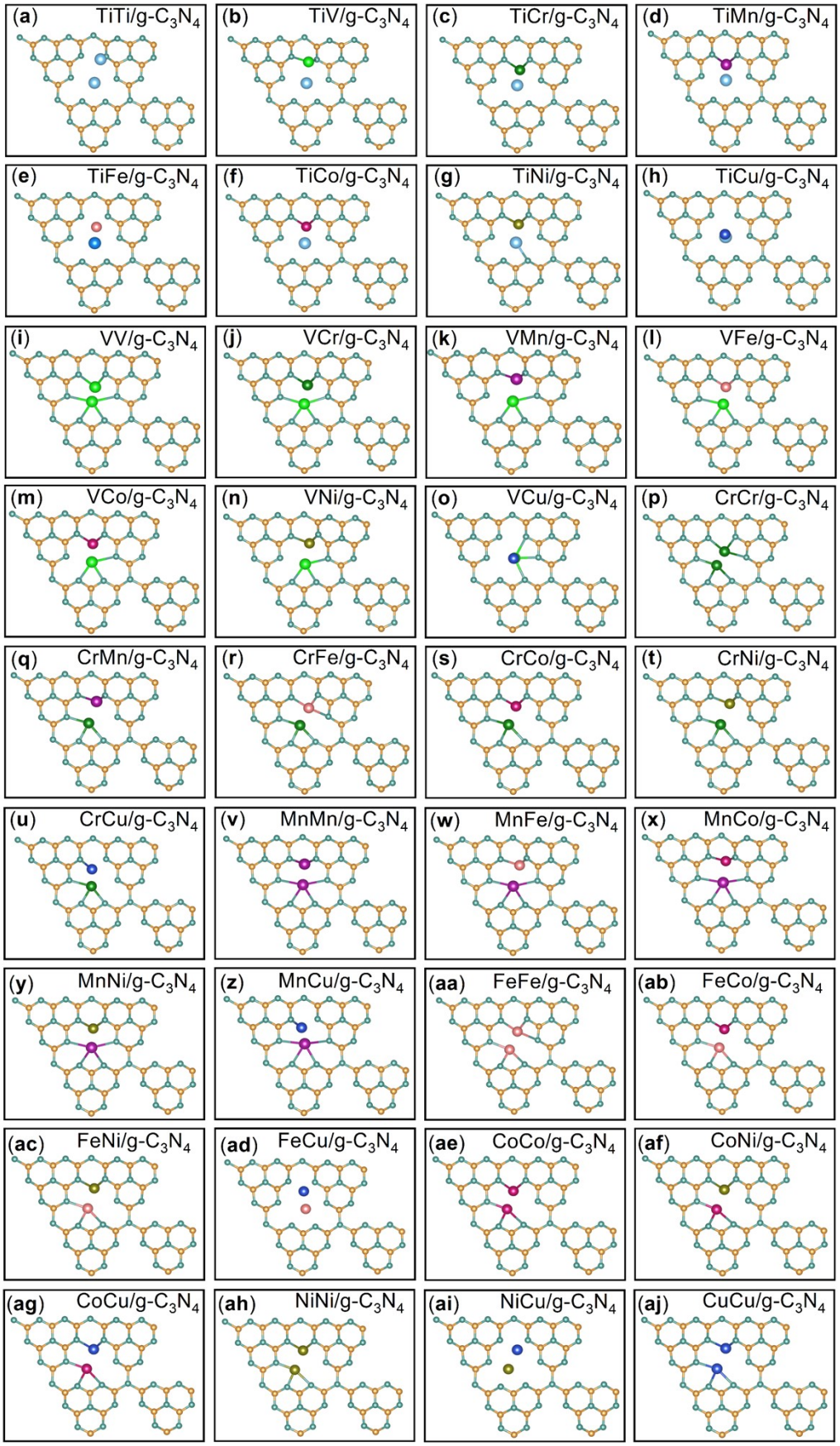

Figure S2 The optimized models of M1M2/g-C_3N_4.

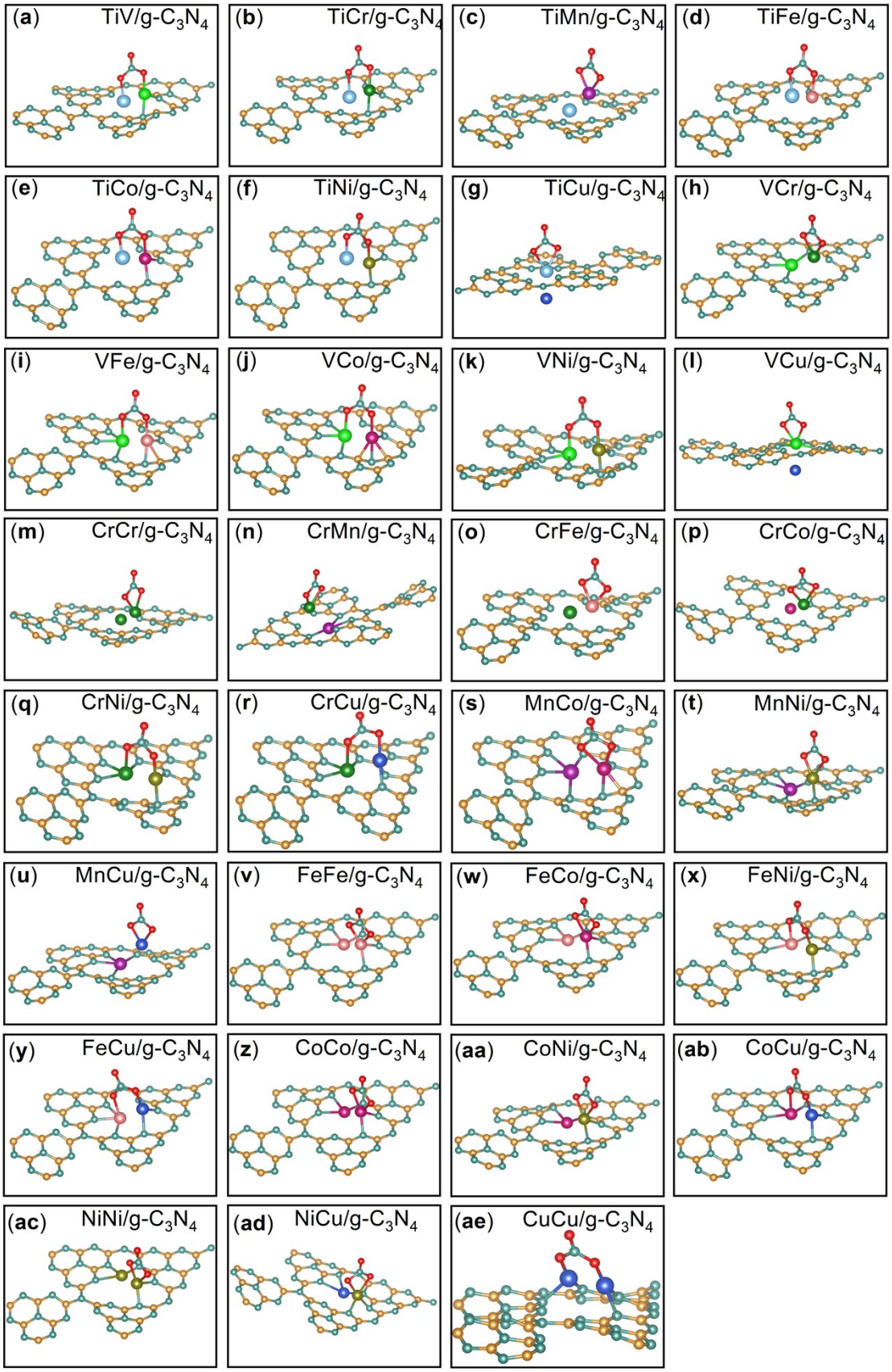

Figure S3 The optimized models of nitrate adsorption on M1M2/g-C_3N_4.

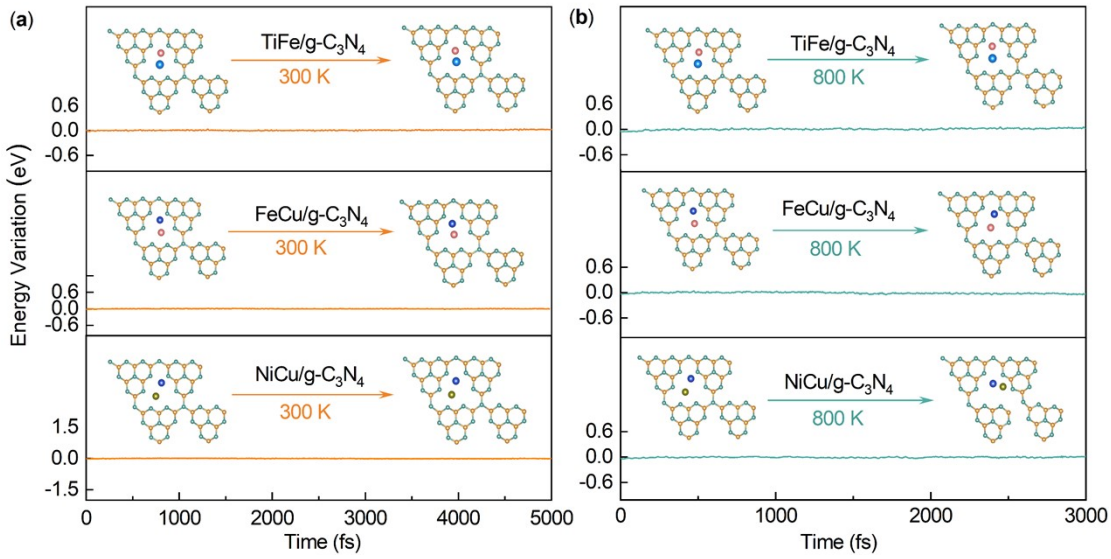

Figure S4. The AIMD of TiFe/g-C_3N_4, FeCu/ g-C_3N_4 and NiCu/ g-C_3N_4 in temperature of a) 300 K and b) 800 K.

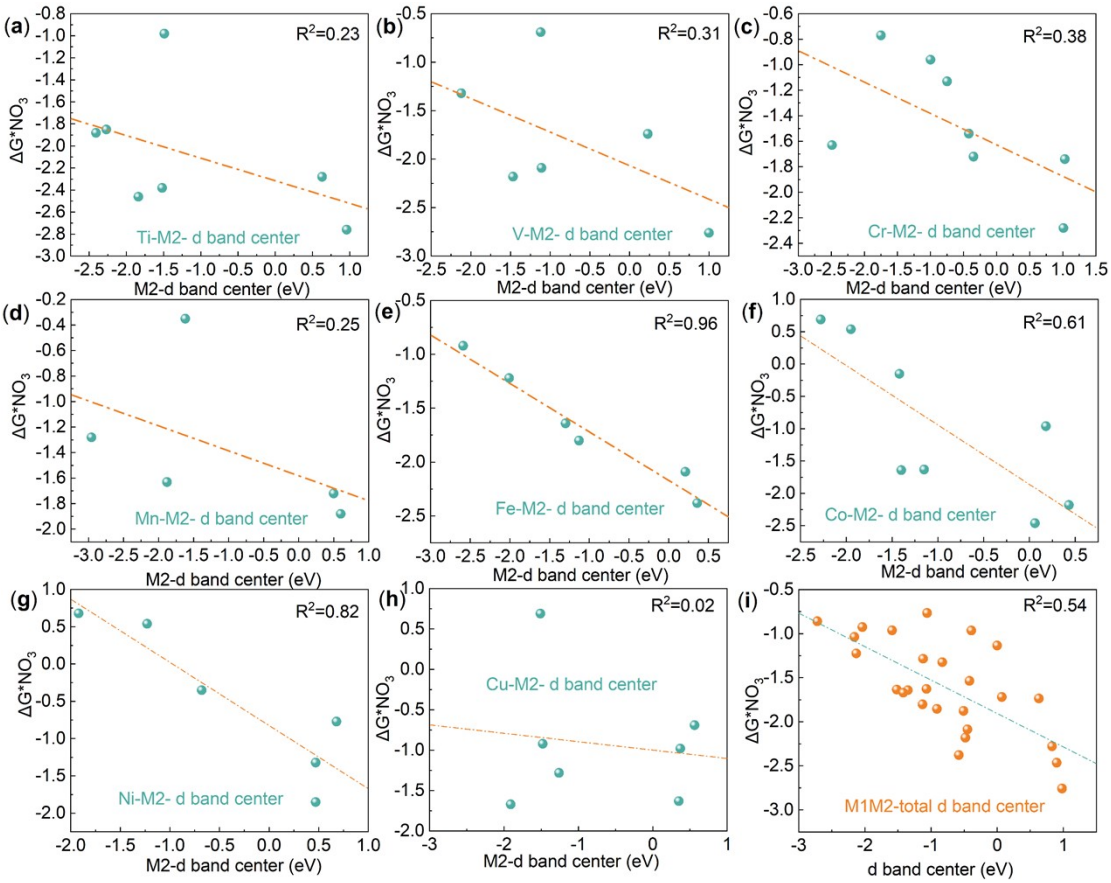

Figure S5. (a)-(h) The relationship of d-band centers of M2 single atom and ΔG^*NO_3, (i) The relationship of d-band centers of M1M2 dual-atoms and ΔG^*NO_3.

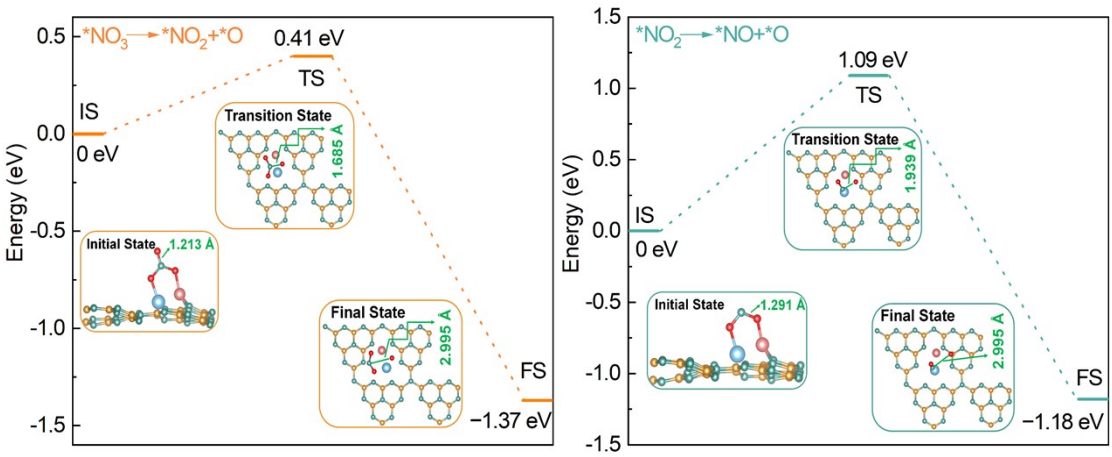

Figure S6. The transition states for TiFe/g-C_3N_4 to perform *NO_3-*NO_2+*O and *NO_2-*NO+*O dissociation reaction.

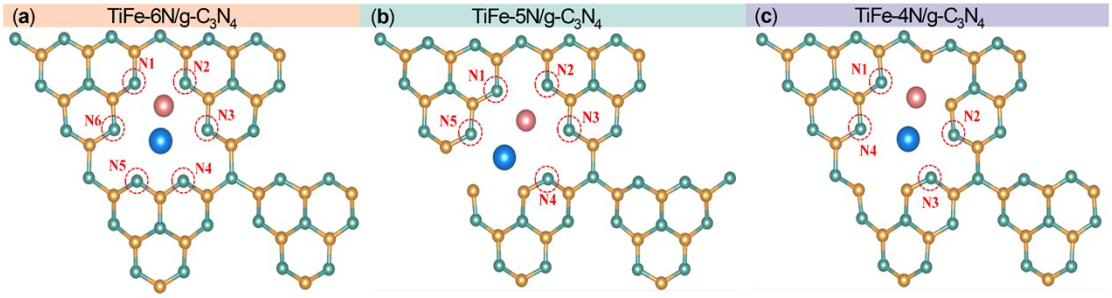

Figure S7. Optimized structure of TiFe coordinated with different N atomic numbers. a) 6 N atoms, b) 5 N atoms and c) 4 N atoms.

REFERENCE

[1] Wang, Y.; Yu, Y.; Jia, R.; Zhang, C.; Zhang, B. Electrochemical Synthesis of Nitric Acid from Air and Ammonia through Waste Utilization. *Natl. Sci. Rev.* 2019, **6**, 730.

[2] Nørskov, J. K.; Rossmeisl, J.; Logadottir, A.; Lindqvist, L.; Kitchin, J. R.; Bligaard, T.; Jónsson, H.; Origin of the Overpotential for Oxygen Reduction at a Fuel-Cell Cathode, *J. Phys. Chem. B* 2004, **108**, 17886-17892.

[3] M. Krack, M. Parrinello, All-electron ab-initio molecular dynamics, *J. Chem. Soc. Faraday Trans.*, 2000, **2**, 2105–2112.

[4] A.D. Becke, A new mixing of Hartree–Fock and local density-functional theories, *J. Chem. Phys.* 1993, **98**, 1372–1377.

[5] B. Delley, Hardness conserving semi local pseudopotentials, *Phys. Rev. B* 2002，**66**, 155125.

[6] G. Di Liberto, L. Giordano, G. Pacchioni, Predicting the Stability of Single-Atom Catalysts in Electrochemical Reactions, *ACS Catal.* 2024, **14**, 45−55.